

Evolution of ultra-relativistic hollow-electron-beam wakefield drivers during their propagation in plasmas

Neeraj Jain¹

*Zentrum für Astronomie und Astrophysik, Technische Universität Berlin,
Hardenbergstr. 36, D-10623, Berlin, Germany^{a)}*

(Dated: 5 July 2021)

Ultra-relativistic hollow electron beams can drive plasma wakefields (\sim GV/m) suitable for positron acceleration. Stable propagation of hollow electron beams for long distances in plasmas is required to accelerate positrons to high energies by these plasma wakefields. In this work, we show by quasi-static kinetic simulations using the code WAKE that an ultra-relativistic azimuthally-symmetric hollow electron beam propagates in a plasma by developing fish-bone like structure and shifting its bulk, differentially along its length (rear part fastest), towards its axis due to the decrease in the betatron time period of beam electrons from the beam-front to beam-rear. Hollow electron beams with small radius collapse into their axis due to the pull by the secondary wakefields generated by some of the beam electrons reaching the axis. Hollow beams with sufficiently large radius, however, can propagate stably in plasmas for several meters and be used for positron acceleration.

^{a)}Max Planck Institute for Solar System Research, Justus-von-Liebig-Weg 3, 37077, Göttingen, Germany

I. INTRODUCTION

Plasma based particle acceleration schemes, first proposed in 1979¹, employ either a high intensity laser or an ultra-relativistic charged particle beam driver which propagates through a plasma driving electromagnetic fields in its wake where charged particles can be accelerated. In the blow-out regime of plasma wake field acceleration^{2,3}, the head of a short electron beam driver expels plasma electrons radially away from its path setting up nonlinear plasma oscillations. The expelled electrons fall back to and cross the beam axis in a tightly confined region behind the beam driver. As a result, the beam driver travels in a plasma-electron-free region which is a bubble-like structure in the moving frame of the beam. A favorable region (longitudinal field accelerating and transverse field focusing) for electron acceleration forms behind the beam driver and inside the first bubble containing the driver. Experiments have demonstrated multi-GeV energy gain of electrons accelerated by plasma wakefields driven by an ultra-relativistic electron beam in the blow-out regime⁴⁻⁸ and also by proton beam⁹. However, acceleration of positrons, which is essential for a successful operation of an electron-positron collider, using plasmas is relatively less explored.

Current schemes of positron acceleration drive plasma wake fields either by electron¹⁰⁻¹² or by positron beam drivers¹³⁻¹⁷. In the blow-out regime driven by electron beam drivers, a narrow favorable region for positron acceleration forms between the first and second bubbles. In the favorable region for positron acceleration, accelerating electric field varies rapidly with axial coordinate leading to a large energy spread in the accelerated witness beam of positrons. An efficient acceleration of positrons in this scheme is possible only if the energy content of the nonlinear plasma waves driven by the electron beam is small¹⁰. In the case of a positron beam driver, plasma electrons are attracted towards rather than expelled out of the beam driver path and do not cross the axis in a confined region as they do in the case of an electron beam driver¹³. As a result the accelerating fields are smaller than those driven by electron beam drivers. The focusing fields are radially nonlinear and vary along the beam axis leading to an emittance growth of the witness positron beam¹⁸. Strength of the accelerating fields and quality of the focusing forces are improved if the positron beam propagates through a hollow plasma channel^{13,15,19}. Misalignment of positron beam from the axis of the hollow plasma channel, however, deflects the beam and sets stringent conditions on the beam alignment²⁰.

A novel scheme using ultra-relativistic hollow electron beams to drive plasma wakefields for positron acceleration was proposed¹². In this scheme, an annular shaped electron free region (bubble) forms generating the wakefields for positron acceleration in the hollow region near the axis of the hollow beam. The accelerating field for positrons in this favorable region of positron acceleration increases with the total charge in the beam driver while the axial size of the favorable region remains approximately of the order of a plasma wavelength which is large enough for the placement of a witness beam of positrons. This is in contrast to the case of a solid beam driver in which the size of the favorable region diminishes with increasing charge in the beam driver. Plasma wakefields for positron acceleration similar to those driven by a hollow electron beam can also be driven by Laguerre-Gaussian laser pulses²¹.

Hollow electron beams with energies in the range from tens to hundreds of MeV have been observed to form in experiments and simulations of laser wake field acceleration^{22–26}. These beams form as a result of the trapping of the self or externally injected electrons in the laser driven plasma wake fields and are of interest for their applications to compact radiation sources. For applications to positron acceleration to high energies, ultra-relativistic hollow electron beam wakefield drivers with large energy contents, of the order of tens of GeV and larger, are of particular interest. Their stable propagation in plasmas for long distances is desirable for the success of their application to positron acceleration. Azimuthally symmetric 2-D simulations demonstrated stable propagation of a hollow electron beam with 23 GeV energy in a plasma for certain plasma and beam parameters, accelerating a positron beam (total charge 13.58 pC) to gain 12.4 GeV in 140 cm¹². Stable propagation of hollow electron beam, however, depends on the parameters (plasma density, beam radius, thickness and charge) which are subjected to variation under optimization of future experiments. In this paper we study evolution of an ultra-relativistic hollow electron beam driver propagating in a plasma and its dependence on the beam radius by quasi-static simulations. We find that a hollow electron beam propagates in a plasma by developing fish-bone like structure and shifting its bulk towards its axis. Hollow beams with small radius collapse into their axis while those with sufficiently large radius can propagate stably in plasmas.

The paper is organized as follows. Section II presents simulation setup for our studies. Evolution of hollow electron beams is discussed in Section III and its dependence on hollow beam radius in Section IV. Finally conclusion are presented in section V.

II. 2-D QUASI-STATIC SIMULATIONS

We simulate propagation of hollow electron beams in uniform plasmas in an azimuthally symmetric ($\partial/\partial\theta = 0$) cylindrical geometry (r, θ, z) using the quasi-static code WAKE^{27,28}. Quasi-static approximation exploits the disparity of the time scales of evolution of plasma and beam driver. The time scale of evolution of an ultra-relativistic electron beam driver (relativistic factor $\gamma_b \gg 1$) is the betatron period $\tau_b = \sqrt{2\gamma_b}\lambda_p/c$ which is much larger than the plasma time scale λ_p/c , where $\lambda_p = 2\pi c/\omega_p$ is the plasma wavelength, c is the speed of light and ω_p is the electron plasma frequency. In the code WAKE, fast response of the kinetic, warm and relativistic plasma to the beam driver is calculated by solving quasi-static equations²⁸ for the wakefields and plasma electrons assuming a non-evolving beam driver in a computational domain which changes its position in the direction of the beam propagation with the beam. The beam driver is then evolved under the influence of the plasma wakefields by solving the equations of motion for beam particles over longer time scales.

We use transverse Coulomb gauge under which azimuthally symmetric electromagnetic fields are described by the electrostatic potential ϕ and vector potential $\mathbf{A} = (0, 0, A_z)$. Quasi-static equations²⁸ for plasma electrons and wakefields can be derived by making the mathematical transformations, $\xi = ct - z$ and $s = z$, and the approximation $\partial/\partial s \ll \partial/\partial\xi$. Under quasi-static approximation, axial and radial wakefields, E_z and $E_{rad} = E_r - cB_\theta$, respectively, can be obtained from the wakefield potential $\psi = \phi - cA_z$ as $E_z = \partial\psi/\partial\xi$ and $E_{rad} = -\partial\psi/\partial r$.

We take initial number density of the hollow electron beam driver as,

$$n_b = n_{b0} \exp \left[-\frac{(r - r_0)^2}{2\sigma_r^2} - \frac{(\xi - \xi_0)^2}{2\sigma_z^2} \right] \quad (1)$$

The peak number density (n_{b0}) of the hollow beam is located at an off axis location (r_0, ξ_0) and falls off within distances σ_r (radially) and σ_z (axially). The beam is completely hollow in the limit $r_0/\sigma_r \rightarrow \infty$. Otherwise there is a small but finite density in the core of the beam. In the limit $r_0 \rightarrow 0$, the beam density has peak at the axis and corresponds to a solid beam.

The background plasma has a uniform density, $n_{p0} = 5 \times 10^{16} \text{ cm}^{-3}$ giving $k_p^{-1} = \omega_p/c = 23.79 \mu\text{m}$, and is modeled using 9 simulation particles per cell. The parameters for electron beam driver are $n_{b0} = n_{p0}$, $\xi_0 = 0$, $\sigma_z = 23.79 \mu\text{m} = k_p^{-1}$, $\sigma_r = 4.76 \mu\text{m} = 0.2k_p^{-1}$. We shall

vary the hollow beam radius r_0 . The total charge $Q_d = -e \int n_b(r, \xi) r dr d\theta d\xi$ contained in the beam driver will thus vary with r_0 . The driver beam has initial energy of 23 GeV and is modeled using 1.25×10^6 simulation particles. The simulation domain size along ξ is approximately $262 \mu\text{m} \approx 11 k_p^{-1}$ with a grid resolution $d\xi = 0.52 \mu\text{m} \approx 0.02 k_p^{-1}$. The simulation domain size and grid resolution in radial direction are approximately $119 \mu\text{m} \approx 5 k_p^{-1}$ and $dr \approx 0.3 \mu\text{m} \approx 0.0125 k_p^{-1}$, respectively. The driver beam is propagated in the uniform plasma in small steps of propagation distance $ds \approx 4.75 \mu\text{m}$.

III. EVOLUTION OF HOLLOW ELECTRON BEAMS

Figs. 1 and 2 show evolution of an ultra-relativistic hollow electron beam driver with radius $r_0 = 8 \sigma_r = 1.6 k_p^{-1}$. The hollow beam develops fish-bone like structure, shifts its bulk towards its axis and finally collapses into its axis during its propagation in a plasma under the influence of the plasma wakefields it drives. Plasma wakefields driven by the initial beam density play an important role in the evolution of the beam and thus we discuss them first.

A. Plasma wake-fields driven by the initial hollow beam density

Propagation of a hollow electron beam driver, density profile given by Eq. (1) and shown in Figs. 1a & 2a, in a plasma causes radial expulsion of the plasma electrons from the beam towards and away from the beam axis at $r = 0$ ¹². Plasma ions pull back the expelled electrons which fall back behind the beam driver forming an azimuthally symmetric annular shape positively charged region in the moving computational domain, as shown in Fig. 1a. The positively charged annular region is bounded by closely spaced trajectories of plasma electrons, and thus plasma charge density ρ_p is negative near (but outside) the radial boundaries of the annular region; the negative values being more pronounced towards the beam-rear as can be seen in radial line-outs of ρ_p at $k_p\xi = -1$ (in the beam-front), $k_p\xi = 0$ (beam center) and $k_p\xi = 2$ (beam-rear) in Fig. 1b. The resulting radial wakefield $E_{rad} = E_r - cB_\theta$ changes direction across the bulk of the beam (Fig. 2a and 2b). Note that slope of a radial line-out of E_{rad} , Fig. 2b, at a radial position where $E_{rad} = 0$ increases towards beam-rear.

Above the upper boundary, ρ_p reaches a negative peak value and then drops to vanish.

Below the lower boundary, on the other hand, ρ_p tends to be radially uniform towards the beam axis after a small drop from its negative peak at the lower boundary. The difference in magnitude and radial variation of ρ_p above and below the upper and lower boundaries, respectively, is because plasma electrons moving towards the beam axis through the beam's hollow region repel each other, and thus are less radially deflected than those moving away from the axis. This makes the annular region radially asymmetric with respect to the beam center at $r = r_0$. Due to the radial asymmetry, the radial location of $E_{rad} = 0$ with respect to the beam center is slightly shifted towards the beam axis (Fig. 2a and 2b).

B. Development of fish-bone like structure in the hollow beam

Fig. 1 shows that the hollow beam driver, which initially had bi-Gaussian shape (Fig. 1a), develops fish-bone like structure by the time it propagates 10 cm into plasma (Fig. 1d). The structure develops as a result of the ξ -dependent time period of the betatron oscillations of the beam electrons. The betatron oscillations are caused by the radial wakefield E_{rad} which acts on beam electrons as a restoring force about the equilibrium positions where $E_{rad}=0$. The betatron time period τ_β under the influence of E_{rad} , whose radial variation near the equilibrium position in a ξ -slice can be approximated as linear (at least for first few tens of centimeters of propagation, Figs. 2b and 2e), can be written as

$$\tau_\beta = 2\pi \sqrt{\frac{m_e \gamma_b}{e [dE_{rad}/dr]_{E_{rad}=0}}} \quad (2)$$

Here $[dE_{rad}/dr]_{E_{rad}=0}$ is the ξ -dependent slope of a radial line-out of E_{rad} at the equilibrium position, γ_b the relativistic factor of the beam particles, m_e the electron's rest mass and e the electronic charge. For a uniform region of ions, Gauss law gives $dE_{rad}/dr = n_{p0}e/2\epsilon_0$ and Eq. (2) reduces to the usual expression $\tau_\beta = \sqrt{2} \gamma_b \lambda_p / c$ for the betatron time period.

Fig. 3a shows dependence of τ_β on ξ at different propagation distances s . We used initial value of γ_b in Eq. (2) for the calculation of τ_β as the axial wake field $E_z \sim 5$ GV/m (not shown here) decelerating the beam reduces the initial beam energy of 23 GeV by a small amount $\sim eE_z \times 10 \text{ cm} = 0.5 \text{ GeV}$ in first 10 cm of propagation. By the time $\Delta t_{10\text{cm}} = 10 \text{ cm}/c \approx 4.2 \times 10^3 / \omega_p$ the beam propagated 10 cm in the plasma developing fish-bone like structure, average change in τ_β from its initial value (at $s=0$ cm) is relatively small (Fig. 3a). On the other hand, τ_β changes by an order of magnitude from the front to

the rear of the beam. It drops from its value $\omega_p \tau_\beta^{front} \approx 10^4$ in the beam front ($k_p \xi = -2$) to reach an asymptotic value $\omega_p \tau_\beta^{rear} = 1.5 \times 10^3$ in the beam rear ($k_p \xi = 2$). Consequently, the beam electrons in different ξ -slices will be in different phases of the oscillations at a given propagation distance s as shown in Fig. 3b. For example, by the time $\Delta t_{10\text{cm}}$, the electrons in the beam-rear with their initial axial positions at $k_p \xi = 1$ and 2, for which values of τ_β are only slightly different, are about to complete their third oscillation ($\Delta t_{10\text{cm}}/\tau_\beta^{rear} \approx 2.8$) while those in the beam-front with initial axial position at $k_p \xi = -2$ are only approximately halfway of their first oscillation ($\Delta t_{10\text{cm}}/\tau_\beta^{front} \approx 0.42$).

Since the beam electrons in neighboring ξ -slices are in different phases of their radial oscillations, the beam density, which at a point (r, ξ) has contributions from neighboring electrons including those in the neighboring ξ -slices, develops a structure different from its initial bi-Gaussian structure. The new structure would depend on the nature of the variation of phases with ξ . In the beam-rear where the ξ -dependence of τ_β and thus of oscillation phase is relatively flat, the beam electrons, for example those with the initial axial positions at $k_p \xi = 1$ and $k_p \xi = 2$ shown in Fig. 3b, oscillate with almost similar phases (at least up to $s=10$ cm) resulting in a beam-rear relatively stretched in ξ . On the other hand, faster variation of τ_β with ξ towards the beam-front results in the development of fish-bone like structure in which wings separated by intervals of pinched beam develop from the front to the rear of the beam. The pinched parts of the beam appears as multiple peaks in beam charge density shown in Fig. 3a. Note that the beam electrons do not significantly change their ξ -positions during the beam propagation, as can be seen from Fig. 3b. Thus moving of the beam electrons to the neighboring slice is not the reason for the fish-bone like structure as may appear from the wings of the structure.

After propagating a finite distance in plasma, the peaks in beam charge density, Fig. 3a, are enhanced over the initial single peak value. The first enhanced peak in the beam front, for example at $k_p \xi \approx -1.75$ at $s=5$ cm, causes much stronger expulsion of the plasma electrons from the beam path than that by the initial beam density, augmenting the positive charge density of plasma behind the peak due to the enhanced exposition of the background ions. As a result, $[dE_{rad}/dr]_{E_{rad}=0}$, which has positive correlation and for $k_p \xi < 2$ linear scaling with $[\rho_p]_{E_{rad}=0}$ as $(e/m_e \omega_p^2)[dE_{rad}/dr]_{E_{rad}=0} = 0.8 [\rho_p/n_{p0}e]_{E_{rad}=0}$ (Fig. 3d) — a reminiscent of the formula $dE_{rad}/dr = \rho_p/2\epsilon_0$ for a uniform background of ions, increases. This cause a local drop in the value of τ_β according to Eq. (2), which appears behind the first enhanced

peak as an ankle-like shape in the τ_β -vs.- ξ curves (Fig. 3a). Since beam density in a given ξ -slice oscillates with s , the first peak at $s=5$ cm subsides and a new first peak at $k_p\xi \approx -2.3$ with a corresponding ankle in τ_β -vs.- ξ curve behind it forms by $s=10$ cm. The value of τ_β drops at other ξ -locations as well but by small amount and does not seem to be associated with the peaks of the beam density. In fact, τ_β at a given ξ oscillates with s in such a way that its maximum value does not exceed its initial value, Fig. 3c.

C. Differential shifting of the beam's bulk towards its axis

Simultaneous with the development of fish-bone structure, the hollow beam shifts its bulk, rear part fastest, towards the beam axis as shown in Fig. 1. The shift results from the betatron oscillations of the beam electrons about an equilibrium position ($E_{rad} = 0$) which shifts radially towards the beam axis during beam propagation. Fig. 4 shows radial oscillations of select beam particles and the changing radial position r_{eq} of the equilibrium at locations in the beam front ($k_p\xi = -1$) and beam rear ($k_p\xi = 1$) as a function of distance s traveled by the beam. At $s = 0$, equilibrium position $k_p r_{eq,0} = 1.5$ is already radially shifted towards the beam axis with respect to the peak beam density at $k_p r = k_p r_0 = 1.6$. This shift is same for all ξ -coordinates as can be noticed in Fig. 2a.

As beam begins to propagate in plasma, beam electrons in a given ξ -slice oscillate about the initial shifted equilibrium position to reach the equilibrium simultaneously, and thus form a density peak there, after approximately a quarter of their first betatron oscillation in that ξ -slice. The density peak forms faster in the rear part of the beam as the betatron oscillations are faster there. Consequently, initially hollow beam takes an overall shape of a conical frustum with the radius decreasing from front to the rear of the beam. Since the effective beam radii for all ξ are now less than the initial beam radius r_0 , propagation of now frustum-shape beam drives wake fields with the equilibrium position further shifted towards the beam axis. Indeed, Fig. 4 shows that the equilibrium position begins to shift towards the beam axis after approximately a quarter of the first betatron oscillations in a given ξ -slice. As the frustum shape beam propagates further, beam electrons adjust to oscillate about the new equilibrium position forming the density peak there and the process continues until the beam reaches too close to the axis. In this way, bulk of the beam shifts towards the axis.

Note that only the beam electrons close to the equilibrium position performs betatron oscillation about the changing equilibrium position. This is because E_{rad} can be approximated as linear only in the neighborhood of the equilibrium position. Away from the equilibrium positions, E_{rad} is nonlinear in r and particle motion is no longer a simple betatron motion.

D. Collapse of the hollow beam into its axis

Figs. 1 & 2 show that the beam finally collapses into its axis. The reason for the collapse is the interaction of the beam electrons with the wakefields generated near the beam axis by some of the beam particles reaching the axis. Fig. 1d or 2d shows that by $s = 10$ cm beam density has already got accumulated on the axis mainly in the region $-1.5 < k_p \xi < 0$. This accumulation is due to the beam electrons reaching the axis in the course of their motion under the influence of the radial force, $F_{rad} = -e E_{rad} = -e \partial(-\psi)/\partial r$, where $\psi(r, \xi, t) = \phi - cA_z$ is the space and time dependent wake field potential. Energy of the radial electron motion,

$$W_r = \frac{\gamma_b m_e v_r^2}{2} + e(-\psi) \quad (3)$$

can be shown to be approximately constant under the assumption of slow time variations of γ_b , ψ and electron's axial position ξ_b . These assumptions are met for a few tens of centimeters of beam propagation.

Figs. 5a and 5b show negative of the wake field potential ($-\psi$) at $s = 0$. Since $\psi = 0$ on the beam axis and initial radial velocities of the beam electrons are zero, only the beam electrons at initial radial positions where $-\psi \geq 0$ can reach the axis. On the other hand, the beam electrons with positive values of ψ significantly different from zero will not reach the axis. Fig. 5c shows that there are small but finite number of particles for which $-\psi \geq 0$. Histogram of the ξ -positions of these particles, Fig. 5d, shows that they are distributed along the whole length of the beam from its front to rear but are mainly concentrated at the axial positions in the range $-1.5 < k_p \xi < 0$ where beam density first accumulates on the axis. Contour of a very small value of $-e\psi/m_e c^2 = 10^{-5}$, which is also closest to the beam in the region $-1.5 < k_p \xi < 0$, show that the particles with $-\psi \geq 0$ are located at the radially outer edge of the beam (Fig. 5a). These particles account for small but finite beam density at the outer beam edge where $|\psi| \approx 0$, as illustrated by radial line-outs of ψ and ρ_b at $k_p \xi = -1$ in Fig. 5b.

Fig. 4 shows that the electrons which have their initial radial positions in the region where $-\psi > 0$ indeed reach close to the axis in the course of their first oscillation. The particles at $k_p\xi = -1$ reach the axis first time around $s=10$ cm later than those at $k_p\xi = 1$ due to their slower oscillations. Since the particles at $k_p\xi = -1$ are larger in number and spend sufficient time $\Delta t = 1\text{cm}/c \approx 420 \omega_{pe}^{-1}$ near the axis, the beam density accumulated on the axis at $k_p\xi = -1$ is larger than that at $k_p\xi = 1$. The on-axis beam density at $k_p\xi = -1$ is also larger than the background plasma density and thus excite secondary wake fields near the axis similar to those excited by a solid electron beam in the blow-out regime, as can be seen by axial line-outs of plasma density and radial wake field in Figs. 1f and 2f. At $s=10$ cm, ρ_p and E_{rad} on the axis are positive over an axial length of the order of a plasma wavelength $2\pi/k_p$ starting around $k_p\xi = -1$. They are not, however, well extended in the radial direction at $s=10$ cm. With the further propagation of the beam, the secondary wake gets radially extended (Figs. 1h and 2h). By $s=30$ cm, beam electrons, which were no reaching the axis, i.e., those with the initial position where $-\psi < 0$, begin to access the radially extended secondary wake field, first in the rear part of the beam, Figs. 1g and 2g. These electrons are pulled by the secondary radial wake field to trap them near the axis, as shown in Fig. 4b. This process continues from the beam-rear to beam-front finally collapsing a significant part of the beam into the axis.

IV. DEPENDENCE ON HOLLOW BEAM RADIUS

Fig. 6 shows mean radial position $\langle r_b \rangle$ of beam electrons, defined at $\xi = \xi_0$ as,

$$\langle r_b \rangle = \frac{1}{N} \sum_{i=1}^N r_{b,i}, \quad \forall i : \xi_0 - d\xi/2 \leq \xi_{b,i} \leq \xi_0 + d\xi/2$$

and radial equilibrium position r_{eq} for $k_p\xi_0 = -1, 1$ and various values of r_0 . Hollow electron beam shifts towards (represented by drops in $\langle r_b \rangle$ and r_{eq} from their initial value) and collapses into its axis (represented by r_{eq} attaining zero value), starting from its rear (Fig. 6b) and progressing towards front (Fig. 6a), for $k_p r_0 = 1.2$ and 1.6 . For larger radii, $k_p r_0 = 1.8$ and 2.0 , hollow beam does shift towards its axis but not collapse even after propagating 200 cms in plasma. Instead, $\langle r_b \rangle$ and r_{eq} simultaneously stop dropping and rise again after a certain propagation distance, e.g., at approximately 120 cm for $k_p r_0 = 2.0$. The rate of drop, distance at which the drop stops and the amount of drop in $\langle r_b \rangle$ and r_{eq}

decrease with the beam radius, resulting in a stable propagation of hollow beam in plasma for large radius, as shown in Fig. 7 for $k_p r_0 = 2.0$.

The reason of no beam collapse for large beam radius can be understood from Fig. 8 which shows negative of the wake field potential ($-\psi$) at $s = 0$ for $k_p r_0 = 2.0$. The contour of $-e\psi/m_e c^2 = 10^{-5}$ in Fig. 8a is fairly away from the beam edges so that the beam density vanishes at the locations where $|\psi| = 0$ (Fig. 8b). Consequently, there are no beam electrons with $-\psi > 0$, as shown in Fig. 8c, to reach and excite secondary wakefields on the axis, avoiding the collapse.

Fig. 7c and 7d shows that a small amount of beam density does accumulate near the axis after propagating a distance $s \sim 100$ cm, much later in comparison to the case of $k_p r_0 = 1.6$. This accumulation of beam density is, however, not due to the beam electrons with $-\psi_{s=0} > 0$ as in the case of $k_p r_0 = 1.6$, but rather due to the evolution of ψ during beam propagation such that some beam electrons have $-\psi > 0$. It, however, disappears by $s = 200$ cm, Figs. 7e and 7f, without affecting the beam propagation. Therefore, number of beam electrons with $-\psi > 0$ at $s = 0$ seems to control the collapse of the beam.

V. CONCLUSION

We have shown by quasi-static kinetic simulations using the code WAKE¹² that an ultra-relativistic hollow electron beam propagates in a plasma by developing fish-bone like structure and shifting its bulk, differentially along its length (rear part fastest), towards its axis. The fish-bone structure develops because electrons performing betatron oscillations in the neighboring beam cross-sections are not in-phase due to the continuous drop of the betatron time period from front to the rear part of the beam. Beam shifts towards its axis due to betatron oscillations of the beam electrons about an equilibrium position which shifts radially towards the beam axis during the beam propagation. The rear part shifts fastest due to the faster betatron oscillations there. For small beam radius, rear part of the beam shifting towards the beam axis is relatively quickly pulled towards the beam axis by the secondary wake fields generated by some of the beam electrons reaching the axis. As a result, hollow beam collapses into its axis with the collapse progressing from its rear to front part. For beams with sufficiently large radius, not many particles reach the axis and the beam can thus propagate stably in plasmas for several meters. For the parameters in our simulations,

beam with radius $k_p r_0 \geq 1.8$ propagates stably up to 200 cms in plasma.

Propagation of ultra-relativistic hollow electron beams in plasmas drive wakefields suitable for positron acceleration (radial field focusing, axial field accelerating) near the beam axis¹². Collapse of the beam into its axis causes the radial wake field near the axis to be defocusing for positrons and thus destroys the wakefield structure for positron acceleration. Hollow electron beams with sufficiently large radius do not collapse but shifts radially towards their axis. The radial shift, however, does not change the wake field structure for positron acceleration. A peak positron accelerating wake field of 2.5 GV/m is produced at the beam axis in our simulations of stable beam propagation with $k_p r_0 = 2.0$. This accelerating field is of the same order of magnitude as observed in experiments of positron acceleration by propagation of positron bunch in hollow plasma channels^{16,17}. Moreover, accelerating field scales linearly with the total charge in the hollow beam driver. Thus, positron acceleration by plasma wakefields driven by hollow electron beams is an attractive scheme for its future application in electron-positron collider.

ACKNOWLEDGMENTS

Author thanks T. M. Antonsen, Jr. (University of Maryland, College Park, MD, USA) for providing the code WAKE. Author thanks T. M. Antonsen and J. P. Palastro (University of Rochester, New York, USA) for initial discussions on the subject.

REFERENCES

- ¹T. Tajima and J. M. Dawson, Phys. Rev. Lett. **43**, 267 (1979).
- ²J. B. Rosenzweig, B. Breizman, T. Katsouleas, and J. J. Su, Phys. Rev. A **44**, R6189 (1991).
- ³W. Lu, C. Huang, M. Zhou, W. B. Mori, and T. Katsouleas, Phys. Rev. Lett. **96**, 165002 (2006).
- ⁴M. J. Hogan, C. D. Barnes, C. E. Clayton, F. J. Decker, S. Deng, P. Emma, C. Huang, R. H. Iverson, D. K. Johnson, C. Joshi, T. Katsouleas, P. Krejcik, W. Lu, K. A. Marsh, W. B. Mori, P. Muggli, C. L. O'Connell, E. Oz, R. H. Siemann, and D. Walz, Phys. Rev. Lett. **95**, 054802 (2005).

- ⁵I. Blumenfeld, C. E. Clayton, F.-J. Decker, M. J. Hogan, C. Huang, R. Ischebeck, R. Iverson, C. Joshi, T. Katsouleas, N. Kirby, W. Lu, K. A. Marsh, W. B. Mori, P. Muggli, E. Oz, R. H. Siemann, D. Walz, and M. Zhou, *Nature* **445**, 741 (2007).
- ⁶M. Litos, E. Adli, W. An, C. I. Clarke, C. E. Clayton, S. Corde, J. P. Delahaye, R. J. England, A. S. Fisher, J. Frederico, S. Gessner, S. Z. Green, M. J. Hogan, C. Joshi, W. Lu, K. A. Marsh, W. B. Mori, P. Muggli, N. Vafaei-Najafabadi, D. Walz, G. White, Z. Wu, V. Yakimenko, and G. Yocky, *Nature* **515**, 92 (2014).
- ⁷S. Corde, E. Adli, J. M. Allen, W. An, C. I. Clarke, B. Clausse, C. E. Clayton, J. P. Delahaye, J. Frederico, S. Gessner, S. Z. Green, M. J. Hogan, C. Joshi, M. Litos, W. Lu, K. A. Marsh, W. B. Mori, N. Vafaei-Najafabadi, D. Walz, and V. Yakimenko, *Nature Communications* **7**, 11898 (2016).
- ⁸C. Joshi, E. Adli, W. An, C. E. Clayton, S. Corde, S. Gessner, M. J. Hogan, M. Litos, W. Lu, K. A. Marsh, W. B. Mori, N. Vafaei-Najafabadi, B. O'shea, X. Xu, G. White, and V. Yakimenko, *Plasma Physics and Controlled Fusion* **60**, 034001 (2018).
- ⁹E. Adli, A. Ahuja, O. Apsimon, R. Apsimon, A.-M. Bachmann, D. Barrientos, F. Batsch, J. Bauche, V. K. Berglyd Olsen, M. Bernardini, T. Bohl, C. Bracco, F. Braunmüller, G. Burt, B. Buttenschön, A. Caldwell, M. Cascella, J. Chappell, E. Chevallay, M. Chung, D. Cooke, H. Damerau, L. Deacon, L. H. Deubner, A. Dexter, S. Doebert, J. Farmer, V. N. Fedosseev, R. Fiorito, R. A. Fonseca, F. Friebel, L. Garolfi, S. Gessner, I. Gorgisyan, A. A. Gorn, E. Granados, O. Grulke, E. Gschwendtner, J. Hansen, A. Helm, J. R. Henderson, M. Hüther, M. Ibison, L. Jensen, S. Jolly, F. Keeble, S.-Y. Kim, F. Kraus, Y. Li, S. Liu, N. Lopes, K. V. Lotov, L. Maricalva Brun, M. Martyanov, S. Mazzoni, D. Medina Godoy, V. A. Minakov, J. Mitchell, J. C. Molendijk, J. T. Moody, M. Moreira, P. Muggli, E. Öz, C. Pasquino, A. Pardons, F. Peña Asmus, K. Pepitone, A. Perera, A. Petrenko, S. Pitman, A. Pukhov, S. Rey, K. Rieger, H. Ruhl, J. S. Schmidt, I. A. Shalimova, P. Sherwood, L. O. Silva, L. Soby, A. P. Sosedkin, R. Speroni, R. I. Spitsyn, P. V. Tuev, M. Turner, F. Velotti, L. Verra, V. A. Verzilov, J. Vieira, C. P. Welsch, B. Williamson, M. Wing, B. Woolley, and G. Xia, *Nature* **561**, 363 (2018).
- ¹⁰K. V. Lotov, *Phys. Plasmas* **14**, 023101 (2007).
- ¹¹X. Wang, R. Ischebeck, P. Muggli, T. Katsouleas, C. Joshi, W. B. Mori, and M. J. Hogan, *Phys. Rev. Lett.* **101**, 124801 (2008).
- ¹²N. Jain, T. M. Antonsen, and J. P. Palastro, *Phys. Rev. Lett.* **115**, 195001 (2015).

- ¹³S. Lee, T. Katsouleas, R. G. Hemker, E. S. Dodd, and W. B. Mori, *Phys. Rev. E* **64**, 045501 (2001).
- ¹⁴B. E. Blue, C. E. Clayton, C. L. O’Connell, F.-J. Decker, M. J. Hogan, C. Huang, R. Iversen, C. Joshi, T. Katsouleas, W. Lu, K. A. Marsh, W. B. Mori, P. Muggli, R. H. Siemann, and D. Walz, *Phys. Rev. Lett.* **90**, 214801 (2003).
- ¹⁵W. D. Kimura, H. M. Milchberg, P. Muggli, X. Li, and W. B. Mori, *Phys. Rev. Lett.* **61**, 90 (2011).
- ¹⁶S. Corde, E. Adli, J. M. Allen, W. An, C. I. Clarke, C. E. Clayton, J. P. Delahaye, J. Frederico, S. Gessner, S. Z. Green, M. J. Hogan, C. Joshi, N. Lipkowitz, M. Litos, W. Lu, K. A. Marsh, W. B. Mori, M. Schmeltz, N. Vafaei-Najafabadi, D. Walz, V. Yakimenko, and G. Yocky, *Nature* **524**, 442 (2015).
- ¹⁷A. Doche, C. Beekman, S. Corde, J. M. Allen, C. I. Clarke, J. Frederico, S. J. Gessner, S. Z. Green, M. J. Hogan, B. O’Shea, V. Yakimenko, W. An, C. E. Clayton, C. Joshi, K. A. Marsh, W. B. Mori, N. Vafaei-Najafabadi, M. D. Litos, E. Adli, C. A. Lindstrøm, and W. Lu, *Scientific Reports* **7**, 14180 (2017).
- ¹⁸P. Muggli, B. E. Blue, C. E. Clayton, F. J. Decker, M. J. Hogan, C. Huang, C. Joshi, T. C. Katsouleas, W. Lu, W. B. Mori, C. L. O’Connell, R. H. Siemann, D. Walz, and M. Zhou, *Phys. Rev. Lett.* **101**, 055001 (2008).
- ¹⁹L. Yi, B. Shen, L. Ji, K. Lotov, A. Sosedkin, XiaomeiZhang, W. Wang, J. Xu, Y. Shi, L. Zhang, and Z. Xu, *Scientific Reports* **4**, 4171 (2014).
- ²⁰C. A. Lindstrøm, E. Adli, J. M. Allen, W. An, C. Beekman, C. I. Clarke, C. E. Clayton, S. Corde, A. Doche, J. Frederico, S. J. Gessner, S. Z. Green, M. J. Hogan, C. Joshi, M. Litos, W. Lu, K. A. Marsh, W. B. Mori, B. D. O’Shea, N. Vafaei-Najafabadi, and V. Yakimenko, *Phys. Rev. Lett.* **120**, 124802 (2018).
- ²¹J. Vleira and J. T. Mendonca, *Phys. Rev. Lett.* **112**, 215001 (2014).
- ²²B. B. Pollock, F. S. Tsung, F. Albert, J. L. Shaw, C. E. Clayton, A. Davidson, N. Lemos, K. A. Marsh, A. Pak, J. E. Ralph, W. B. Mori, and C. Joshi, *Phys. Rev. Lett.* **115**, 055004 (2015).
- ²³T. Z. Zhao, K. Behm, C. F. Dong, X. Davoine, S. Y. Kalmykov, V. Petrov, V. Chvykov, P. Cummings, B. Hou, A. Maksimchuk, J. A. Nees, V. Yanovsky, A. G. R. Thomas, and K. Krushelnick, *Phys. Rev. Lett.* **117**, 094801 (2016).
- ²⁴G.-B. Zhang, M. Chen, J. Luo, M. Zeng, T. Yuan, J.-Y. Yu, Y.-Y. Ma, T.-P. Yu, L.-L.

- Yu, S.-M. Weng, and Z.-M. Sheng, *Journal of Applied Physics* **119**, 103101 (2016).
- ²⁵G.-B. Zhang, M. Chen, C. B. Schroeder, J. Luo, M. Zeng, F.-Y. Li, L.-L. Yu, S.-M. Weng, Y.-Y. Ma, T.-P. Yu, Z.-M. Sheng, and E. Esarey, *Physics of Plasmas* **23**, 033114 (2016).
- ²⁶Z.-C. Shen, M. Chen, G.-B. Zhang, J. Luo, S.-M. Weng, X.-H. Yuan, F. Liu, and Z.-M. Sheng, *Chinese Physics B* **26**, 115204 (2017).
- ²⁷P. Mora and T. M. Antonsen, *Phys. Plasmas* **4**, 217 (1997).
- ²⁸N. Jain, J. Palastro, T. M. Antonsen, W. B. Mori, and W. An, *Physics of Plasmas* **22**, 023103 (2015).

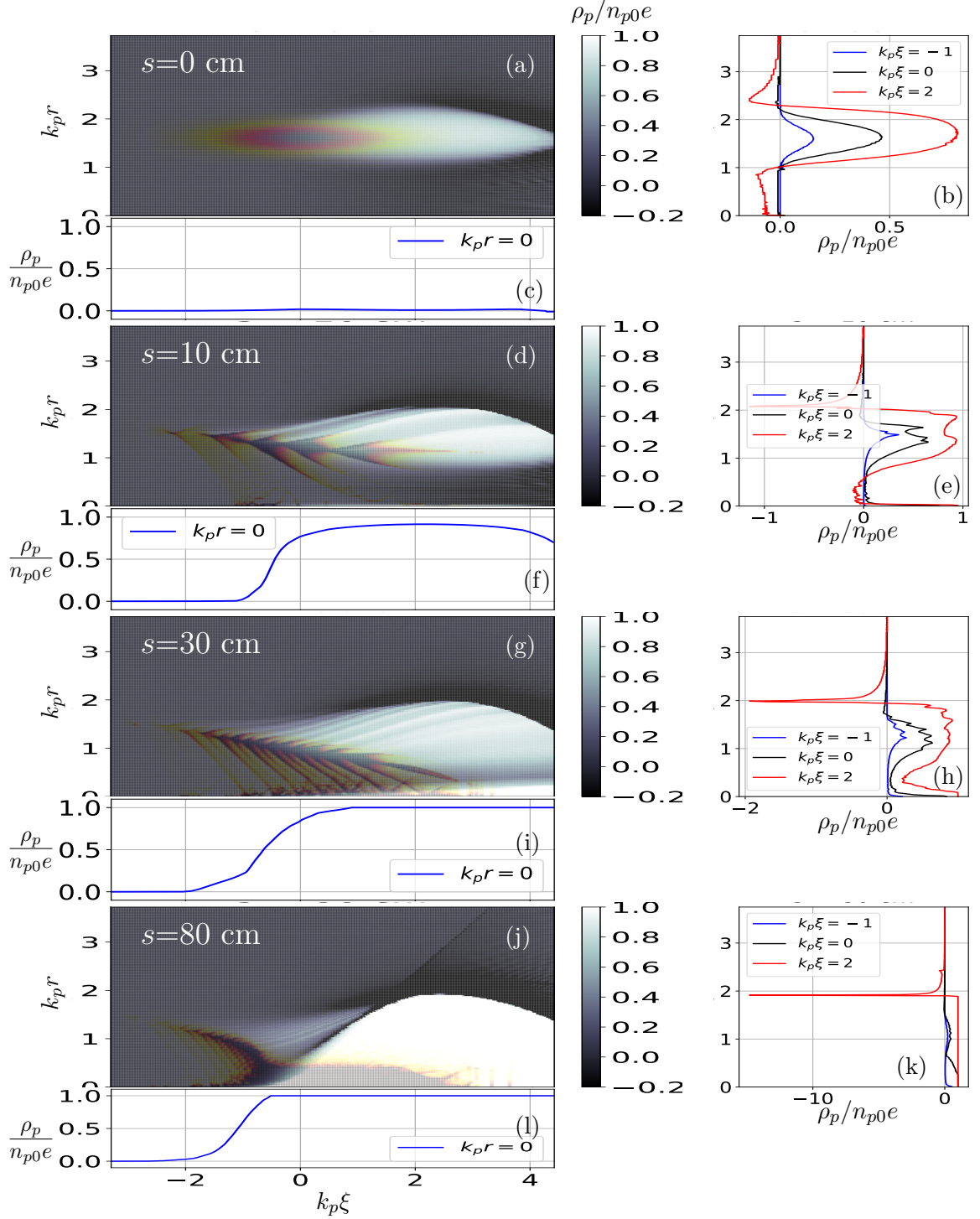


FIG. 1. Plasma charge density $\rho_p/(n_{p0}e)$ (in black-white color map) driven by a hollow electron beam of radius $k_p r_0 = 1.6$ moving towards left, at propagation distances $s=0$ cm (a), 10 cm (d), 30 cm (g) and 80 cm (j). Over-plotted is the beam charge density $\rho_b/(n_{p0}e)$ in black-red-yellow color map saturated at $\rho_b/(n_{p0}e)=-1$. Radial and axial line-outs of ρ_p at a given s are shown on the right of and below the corresponding color plot, respectively.

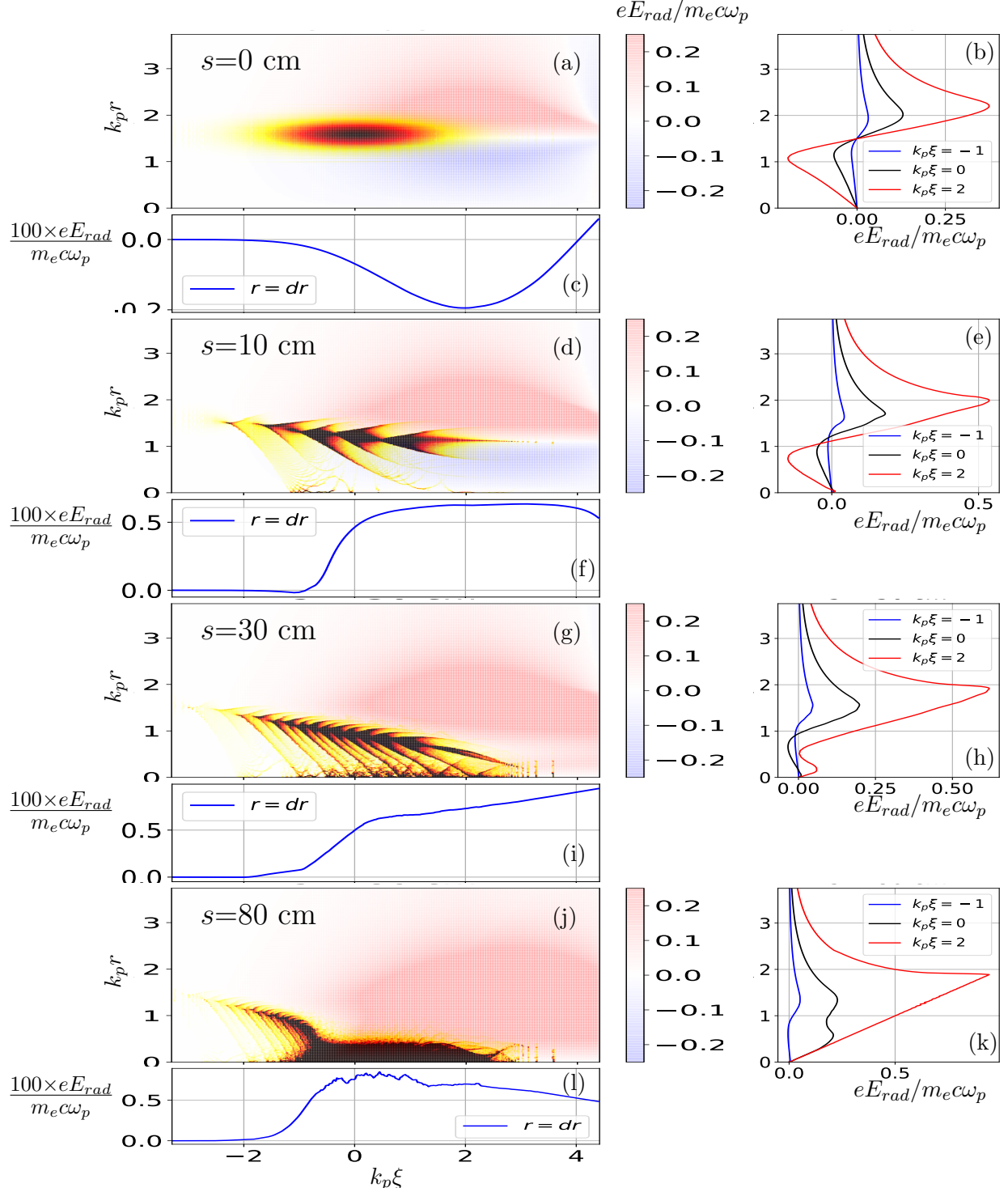


FIG. 2. Radial wakefield $eE_{rad}/m_e c \omega_p$ (in blue-white-red color map) driven by a hollow electron beam of radius $k_p r_0 = 1.6$ moving towards left, at propagation distances $s=0$ cm (a), 10 cm (d), 30 cm (g) and 80 cm (j). Over-plotted is the beam charge density $\rho_b/(n_{p0}e)$ in black-red-yellow color map saturated at $\rho_b/(n_{p0}e)=-1$. Radial and axial line-outs of E_{rad} at a given s are shown on the right of and below the corresponding color plot, respectively.

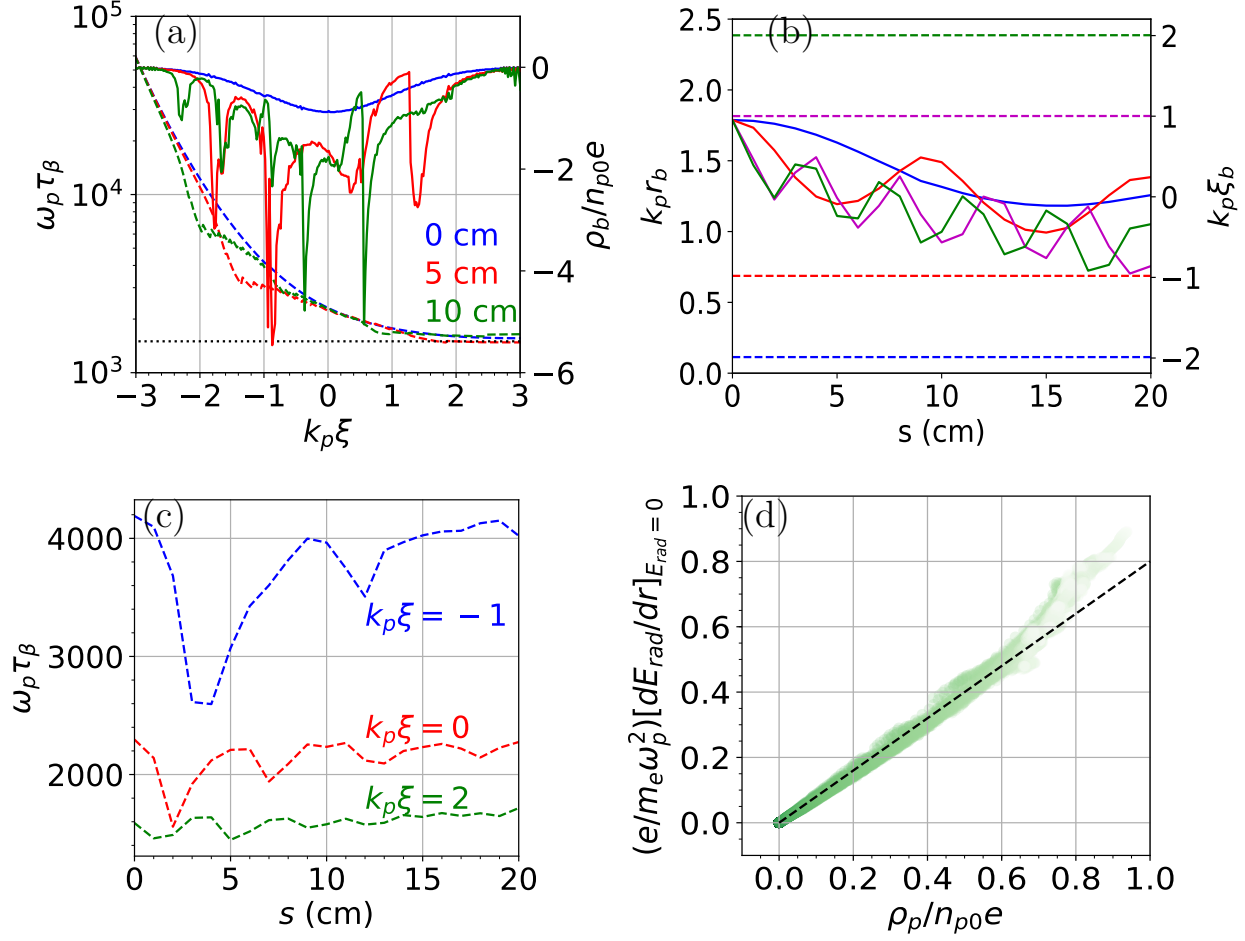


FIG. 3. In (a), betatron time period $\omega_p \tau_\beta$ (left axis, dashed lines) calculated from Eq. (2) using the initial value of γ_b and beam charge density $[\rho_b/(n_{p0}e)]_{E_{rad}=0}$ (right axis, solid lines) vs. $k_p \xi$ at $s = 0$ cm (blue), 5 cm (red) and 10 cm (green). A horizontal dotted line in (a) is for $\omega_p \tau_\beta = 1.5 \times 10^3$. In (b), radial ($k_p r_b$, left axis, solid lines) and axial ($k_p \xi_b$, right axis, dashed lines) positions vs. s for select beam particles with same initial radial $r \approx r_0 + \sigma_r = 1.8k_p^{-1}$ but different axial positions $k_p \xi = -2$ (blue), -1 (red), 1 (magenta) and 2 (green). In (c), $\omega_p \tau_\beta$ vs. s at $k_p \xi = -1$ (blue), $k_p \xi = 0$ (red) and $k_p \xi = 2$ (green). In (d), scatter plot $(e/m_e \omega_p^2)[dE_{rad}/dr]_{E_{rad}=0}$ vs. $[\rho_p/(n_{p0}e)]_{E_{rad}=0}$ for $k_p \xi < 3$ (green color representing ξ -location fades towards the beam-rear) and $s \leq 20$ cm, and a fit $(e/m_e \omega_p^2)[dE_{rad}/dr]_{E_{rad}=0} = 0.8 [\rho_p/(n_{p0}e)]_{E_{rad}=0}$ (dashed line).

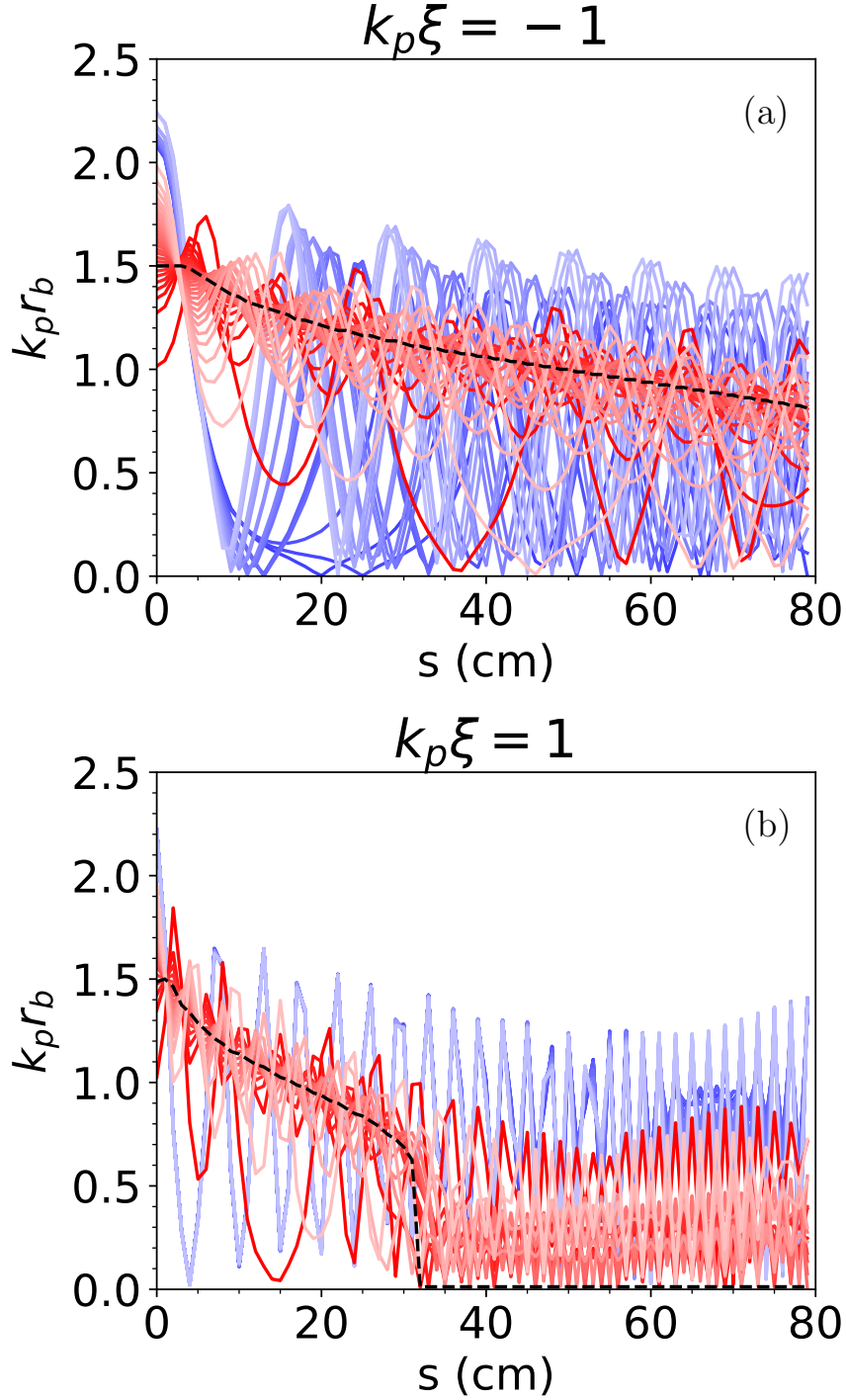


FIG. 4. Radial positions r_b (solid lines) of select beam particles and equilibrium position r_{eq} (dashed line) in the ξ -slices $k_p \xi = -1$ (a) and 1 (b) as a function of the distance s traveled by the beam. Lines with shades of blue (red) represent the particles whose initial radial positions are in the region where $-\psi > 0$ ($-\psi < 0$). Shades are used to distinguish different particles represented by a same color.

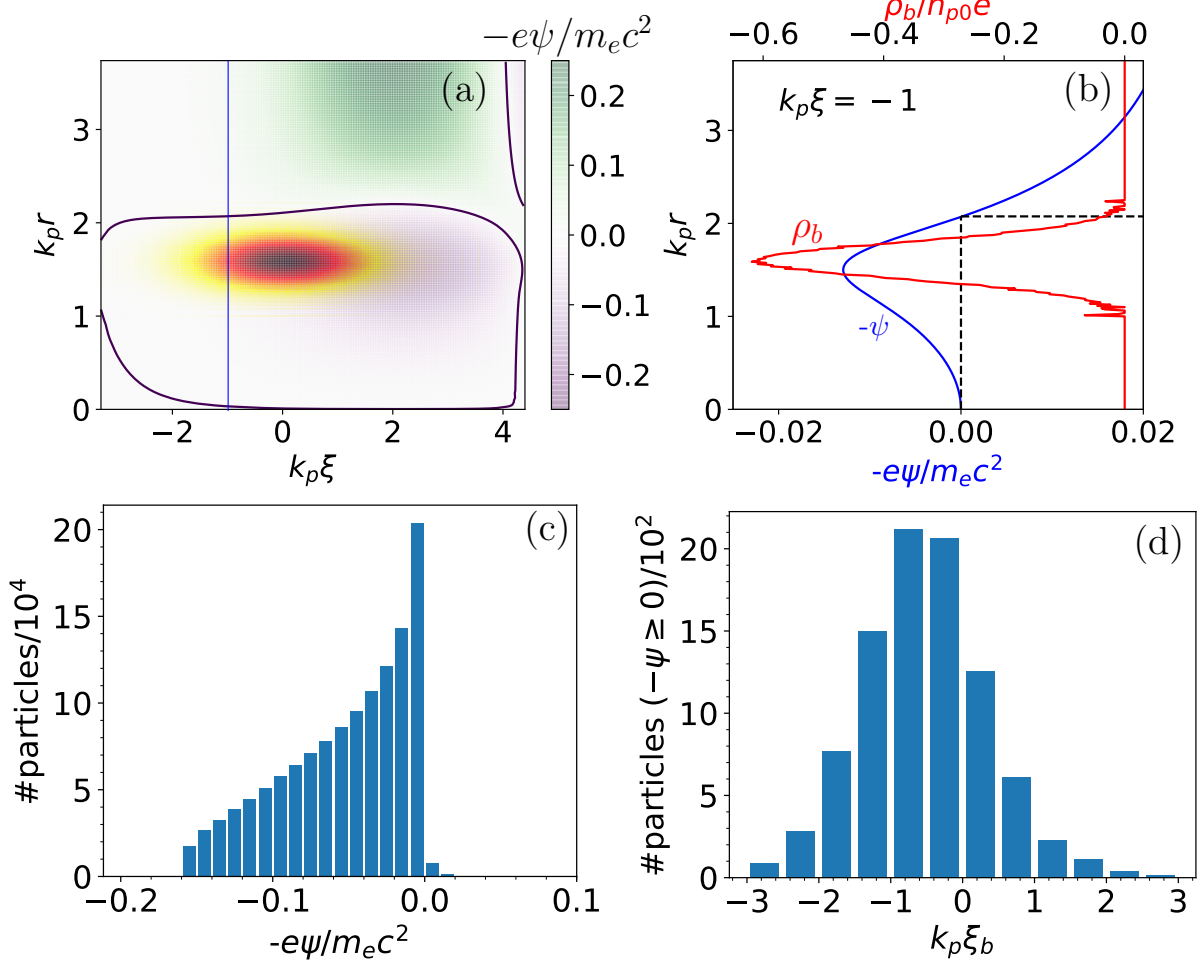


FIG. 5. Negative of wakefield potential, i.e., $-e\psi/m_e c^2$, (purple-green color map), a contour of $-e\psi/m_e c^2 = 10^{-5}$ (black line) and $\rho_b/(n_{p0}e)$ (red-yellow color map) at $s = 0$ (a). Radial line-outs of $\rho_b/(n_{p0}e)$ (red, top horizontal axis) and $-e\psi/m_e c^2$ (blue, bottom horizontal axis) along the blue vertical line drawn in (a) at $k_p \xi = -1$ (b). Horizontal and vertical dashed lines in (b) meet the ψ -curve where $\psi = 0$. Histogram of the values of $-e\psi/m_e c^2$ at particles position (c). Histogram of the ξ -positions of the particles for which $-\psi \geq 0$ (d).

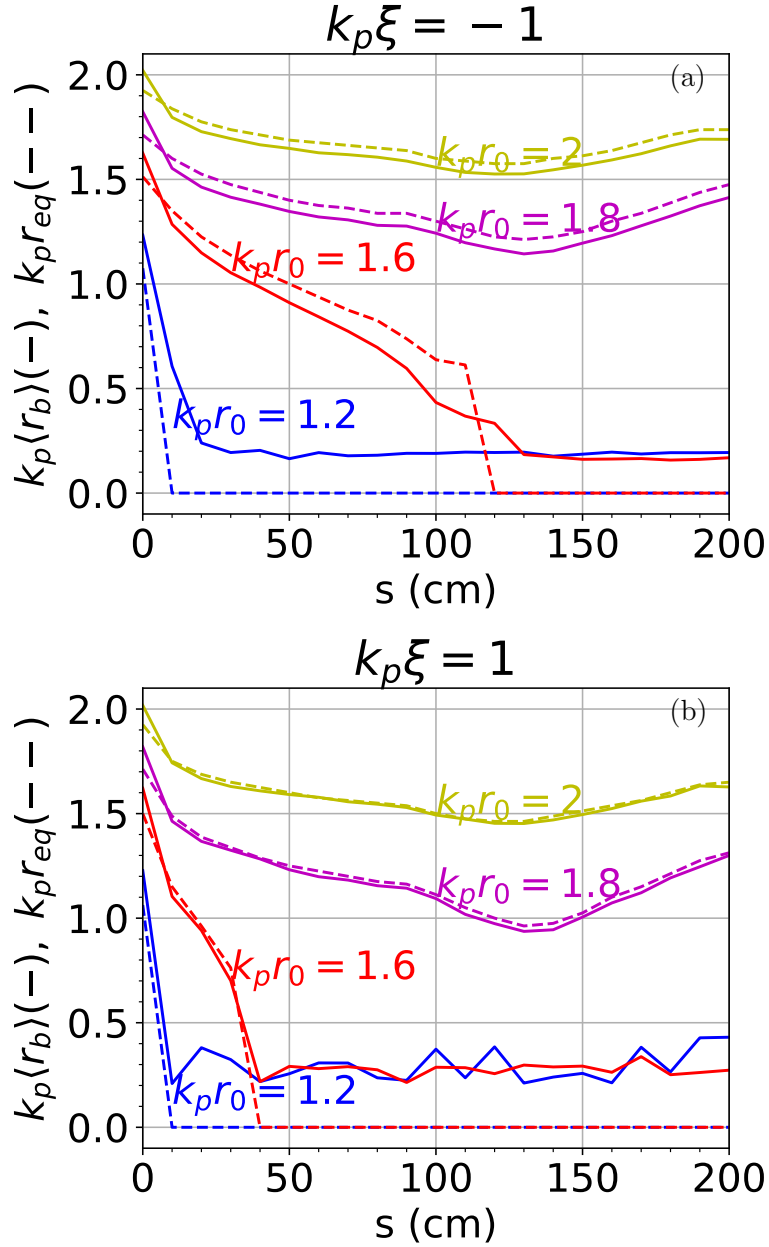


FIG. 6. Mean radial position $\langle r_b \rangle$ of beam electrons (solid line) and radial position r_{eq} of the equilibrium (dashed line) at $k_p \xi = -1$ (a) and $k_p \xi = 1$ (b) as a function of the distance s traveled by the beam for various value of r_0 .

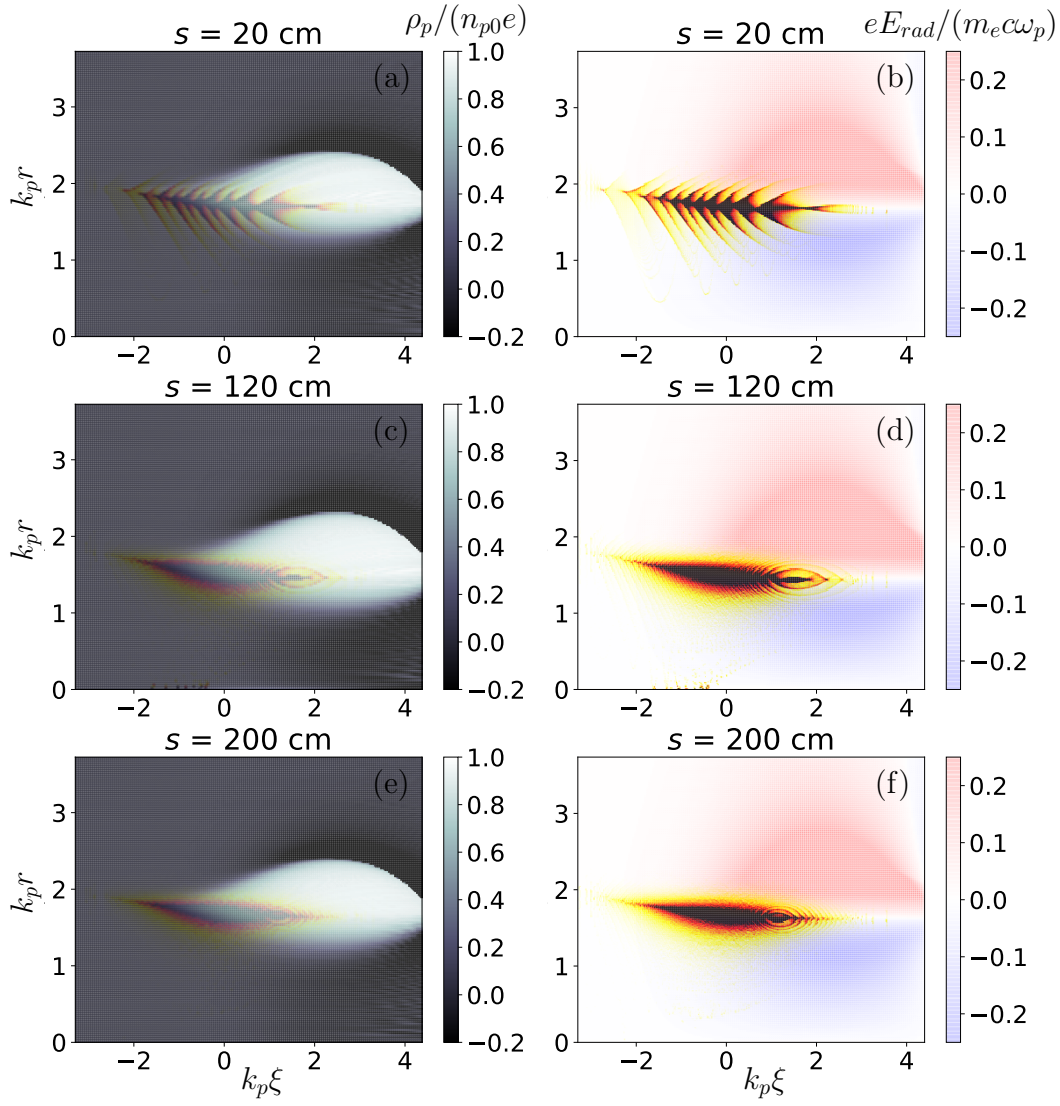


FIG. 7. Plasma charge density $\rho_p/(n_{p0}e)$ (left column, black-white color map) and radial wakefield $eE_{rad}/m_e c \omega_{pe}$ (right column, blue-white-red color map) driven by a hollow electron beam ($n_{b0} = n_p$, $k_{pr0} = 2.0$) moving towards left, at various propagation distances. Over-plotted is the beam charge density $\rho_b/(n_{p0}e)$ in black-red-yellow color map saturated at $\rho_b/(n_{p0}e) = -1$.

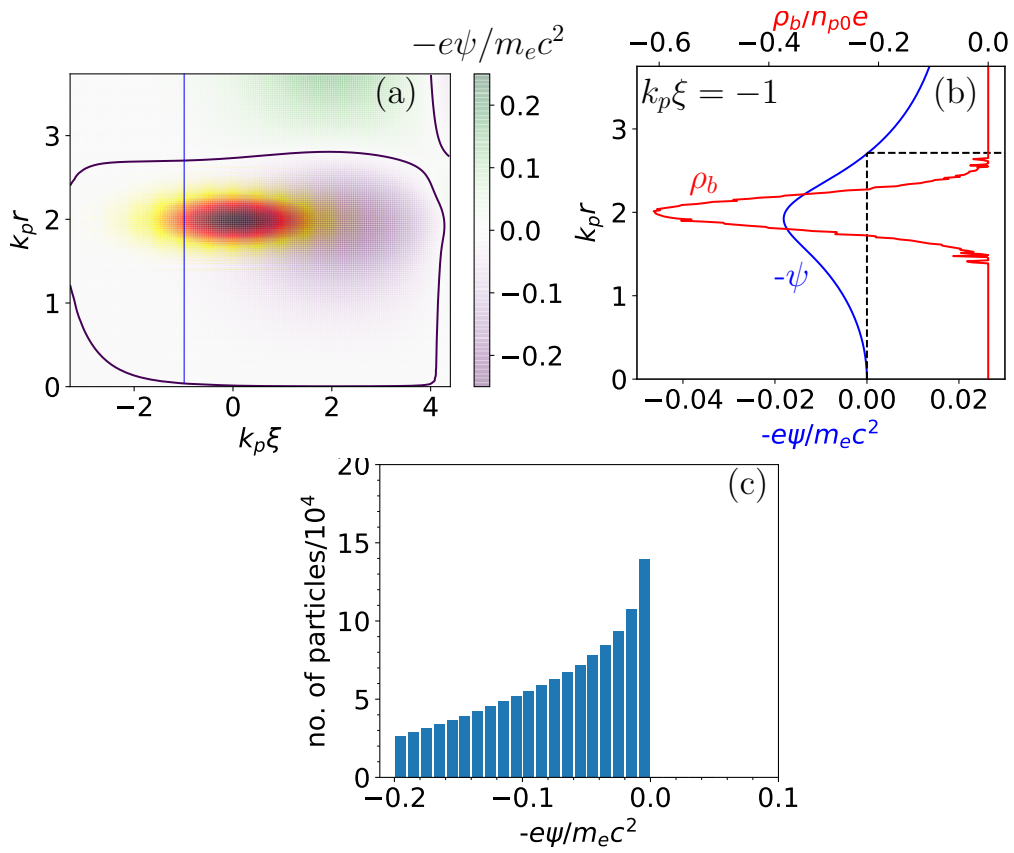


FIG. 8. (a), (b) and (c) are the same as those in Fig. 5 but here for $k_p r_0 = 2.0$.